Phase Evolution, Texture Behavior, and Surface Chemistry of Hydrothermally Derived Scandium (Hydrous) Oxide Nanostructures

Ya-Wen Zhang, Jian-Hua Liu, Rui Si, Zheng-Guang Yan, and Chun-Hua Yan*

State Key Lab of Rare Earth Materials Chemistry and Applications and PKU-HKU Joint Lab on Rare Earth Materials and Bioinorganic Chemistry, Peking University, Beijing 100871, China

Received: April 11, 2005; In Final Form: August 11, 2005

Nanostructured scandium hydrous oxides were hydrothermally synthesized at 180 °C for 18 h, using NaOH, NH_4OH, and KOH as the bases. They were characterized by means of X-ray diffraction (XRD), transmission electron microscopy (TEM), N_2 adsorption, thermogravimetry and differential thermal analysis (TG−DTA), infrared and Raman spectroscopy, and pyridine adsorption. XRD and TEM measurements showed that the nature and concentration of the bases played key roles in determining the phasic composition, texture behavior (shape and size), and surface chemistry of the hydrothermal products. In addition, the shape evolution of the crystalline products seemed to be closely connected with their crystal structures. As the basicity value was raised from pH 10 to 5 mol L^{-1} NaOH (or KOH), α-ScOOH nanorods, α-ScOOH nanosized hexagonal-like plates, and cubic $Sc(OH)_3$ cubes/cuboids in micrometer size were produced in turn; while within pH 10−12 using NH_4OH, γ-ScOOH nanosized lozenge-like plates were mainly obtained. According to XRD, TEM, and TG−DTA results, all the as-prepared nanostructured ScOOH and micrometric $Sc(OH)_3$ could be converted to cubic Sc_2O_3 with sustained crystalline shape via calcination at 500 °C. Pyridine adsorption revealed the existence of Lewis acid sites on the surfaces of the nanostructured α-ScOOH samples and some of their Sc_2O_3 counterparts calcined at 700 °C. The α-ScOOH nanorod sample displayed the strongest Lewis acidity among all the samples tested, due to its highest surface area as determined by N_2 adsorption. Finally, an olation−oxolation process based on a dissolution/recrystallization mechanism accounts for the formation of various ScOOH polymorphs and $Sc(OH)_3$ with different shapes.

1. Introduction

In the last decade, nanostructured inorganic compounds (e.g., elemental semiconductors, II−VI and III−V semiconductors, metals, metal oxides, and inorganic salts) have attracted considerable interest not only because of their unique properties with respect to their bulk materials but also because of their promising applications in catalysis, optics, electronics, optoelectronics, magnetics, biosensing, and therapeutics.[1−7] More recently, nanostructured rare earth (lanthanide, Sc, and Y) compounds, due to their promising applications in magnets, phosphors, catalysts, biochemical probes, and medical diagnostics, have attracted much attention from traditional nanostructured compounds. Efforts have been devoted to the synthesis and characterization of rare earth hydroxides, oxides, borates, fluorides, and phosphates with dimension-controlled nanostructures such as nanoparticles, nanowires, nanorods, and nanotubes.[8−14] However, the advance in the studies on nanostructured scandia compounds is still very limited.

Among the trivalent rare earths, Sc^{3+} has the smallest ionic size and its hydroxide is the most acidic. In particular, scandium oxide possesses a high refractive index ($n_H = 2.0$ at $\lambda = 300$ nm), high band gap (5.7 eV, corresponding to a UV cutoff of 215 nm), and a high melting point (~2485 °C). Sc_2O_3-based materials have favored the applications in catalytic reactions such as NO reduction by CH_4,[15] ionic conductors (stabilized zirconia),[16] high-power pulsed UV lasers, and optical components (mirrors, shields, protective layers, and polarizers).[17,18] Some wet chemical approaches including sol−gel, homogeneous precipitation, and hydrothermal methods have recently been developed to synthesize Sc_2O_3 nanomaterials.[18−20] For example, Grosso and Sermon reported the synthesis of Sc_2O_3 nanoparticles with a size less than 80 nm via a sol−gel route.[18] Ripert et al. prepared nanosized lozenge-shaped platelets of γ-ScOOH by a hydrothermal method.[19] Li et al. investigated the homogeneous precipitation of Sc_2O_3 nanopowders from various inorganic salt precursors.[20] However, there have been no reports of one-dimensional (1D) ScOOH or Sc_2O_3 nanomaterials or systematic investigation into the preparation and characterization of nanostructured scandium (hydrous) oxides. The latter case not only makes it difficult to obtain their requisite nanomaterials of pure phase in a reproducible manner but also has hindered them from finding new applications.

This research aims at synthesizing nanostructured scandium (hydrous) oxides by a hydrothermal method and investigating the effects of various bases and their concentrations on the crystal structure, crystalline shape, calcination behavior, and surface chemistry of the products. Unlike in the cases of the coprecipitation and the sol−gel method, the products of hydrothermal reactions do not require postannealing treatments and are usually highly crystalline with well-defined morphology and high powder reactivity. In this paper, the phase evolution, texture behavior, and surface chemistry of nanostructured scandium (hydrous) oxides hydrothermally synthesized under various basic conditions are presented. Particularly, an olation−oxolation process based on a dissolution/recrystallization mechanism was

* Corresponding author. Phone and Fax: +86-10-62754179. E-mail: yan@pku.edu.cn.

10.1021/jp051870b CCC: $30.25 © 2005 American Chemical Society
Published on Web 09/14/2005

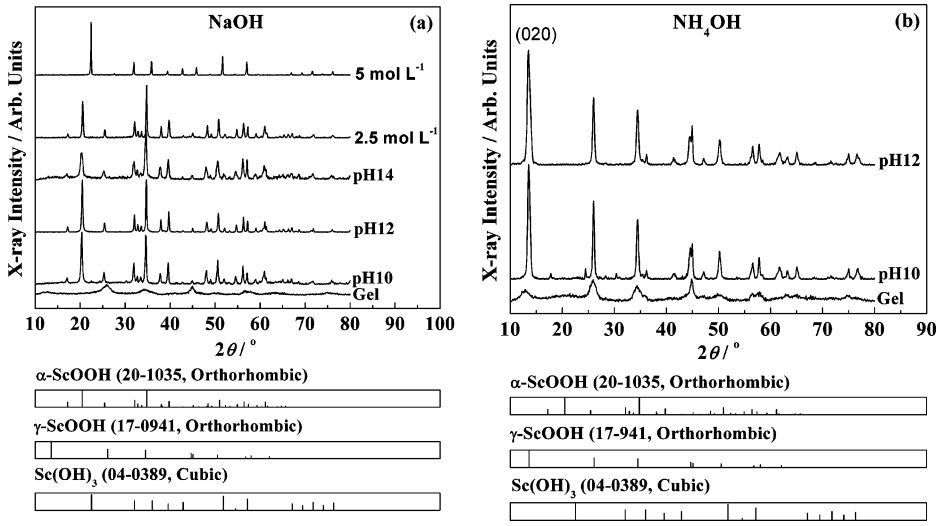

Figure 1. XRD patterns of the samples prepared using (a) NaOH and (b) NH_4OH, and of the corresponding $Sc(OH)_3$ gels.

proposed to explain the formation of various ScOOH polymorphs and $Sc(OH)_3$ with different shapes.

2. Experimental Section

2.1. Synthesis. Sc_2O_3 (> 99.95%, AR, Zhaoqing Nonferrous Metals and Industry Corp., China) was dissolved in hot concentrated HNO_3 (AR, Beijing Chem. Corp., China) to prepare a $Sc(NO_3)_3$ solution. A portion of the $Sc(NO_3)_3$ solution and bases such as NaOH, KOH, or NH_4OH (all AR grade, Beijing Chem. Corp., China) were employed to prepare the stock solution (40 mL) with a Sc^{3+} concentration lying between 0.008 and 0.075 mol L^{-1} in a Teflon bottle (inner volume, 50 mL), which was kept in a stainless steel autoclave. As the base was mixed with the $Sc(NO_3)_3$ solution, milky white precipitates formed promptly. After the basicity of the stock solution had been adjusted to the desired value, the autoclave was sealed tightly and placed in a temperature-controlled electric oven followed by a hydrothermal treatment at temperatures between 120 and 200 °C for 0.5−48 h. After this, white precipitates were separated by centrifugation, washed with deionized water and ethanol several times, and subsequently dried at 60 °C in air overnight. The products were thus obtained with yields of ca. 90% and then were calcined in air at temperatures between 500 and 900 °C for 2−5 h.

2.2. Characterization Methods. Thermogravimetry and differential thermal (TG−DTA) analysis was performed with a Universal V2.60 TA instrument at a heating rate of 10 °C min^{-1} from room temperature to 1000 °C, using α-Al_2O_3 as a reference. Infrared spectra (IR) (4000−400 cm^{-1}) were obtained on a Nicolet Magna 750 FTIR spectrometer at a resolution of 4 cm^{-1} with a Nic-Plan IR microscope (128 scans). Far-IR spectra (650−50 cm^{-1}) were measured on the same spectrometer at a resolution of 8 cm^{-1} with a DTGS/Polyethylene detector (100 scans), using Nujol mulls. Raman spectra were determined on a Nicolet FT Raman 950 spectrometer at a resolution of 8 cm^{-1} (1280 scans).

The powder X-ray diffraction (PXRD) patterns were recorded on a Rigaku D/MAX-2000 diffractometer with a slit of $^1/_2$ deg at a scanning rate of 4 deg min^{-1}, using Cu Kα radiation (λ = 1.5406 Å). The lattice parameters were calculated with the "LAPOD" software of least-squares refinement of cell dimensions from powder data by Cohen's Method.[21,22]

The BET specific surface area (*S*) was measured by nitrogen adsorption at 78.3 K, using an ASAP 2010 analyzer (Micromeritics Co. Ltd.), after degassing the sample at 423 K for at least 4 h under vacuum down to a residual pressure better than 10 μm of Hg. Sample morphologies were probed by transmission electron microscopy (TEM) (200CX, JEOL). High-resolution TEM (HRTEM) characterization was performed with a Philips Tecnai F30 FEG-TEM operated at 300 kV.

The acidities of the samples were determined by the pyridine adsorption technique. Pyridine FTIR spectra were recorded with a BIO-RAD FTS-3000 FTIR spectrometer. The samples were pressed into self-supporting wafers (10 mg cm^{-2} thickness), placed in an IR cell, and treated at 350 °C for 1.5 h under dynamic evacuation of the cell (10^{-3} Pa). After cooling to room temperature, the samples were exposed to pyridine vapor for 10−15 min until equilibration. Then, the spectra (20 scans, 4 cm^{-1} resolution) of the pyridine bonded by the Brønsted and Lewis acid sites were recorded at room temperature after evacuation for 0.5 h at 200 and 350 °C. The acidities of the samples were compared by the value of the integrated absorbance over the mass of the wafer.

3. Results

In the beginning of the synthesis, as a base (NaOH, NH_4OH, or KOH) was added into the Sc^{3+} solution, a milky white precipitate formed promptly. The precipitates were separated by centrifugation, washed with deionized water and ethanol several times, and dried at 60 °C in air overnight; $Sc(OH)_3$ gels were obtained. Whatever the bases used, the white gels were poorly crystallized nanometric γ-ScOOH, which we named pseudo-γ-ScOOH, as indicated by the considerable broadening of the weak diffraction peaks (Figure 1 and Figure 1S in the Supporting Information). We also found that, when the fresh white precipitates were directly subjected to hydrothermal treatment at 180 °C for 18 h, well-shaped ScOOH and $Sc(OH)_3$ crystallites with a high yield (ca. 90%) were obtained under pH > 9 (Figures 1 and 2 and Figures 1S and 2S in the Supporting Information), but irregular-shaped crystalline products with a low yield (<50%) were produced under pH < 9 (Figures 3S and 4S in the Supporting Information). Therefore, all the hydrothermal syntheses were performed at 180 °C for 18 h under pH > 9, for convenience in comparing the experimental results.

3.1. Crystal Structure, Crystalline Shape, and Size. By XRD and TEM, the crystal structures, crystalline shapes, and sizes of the hydrothermal products synthesized at 180 °C for

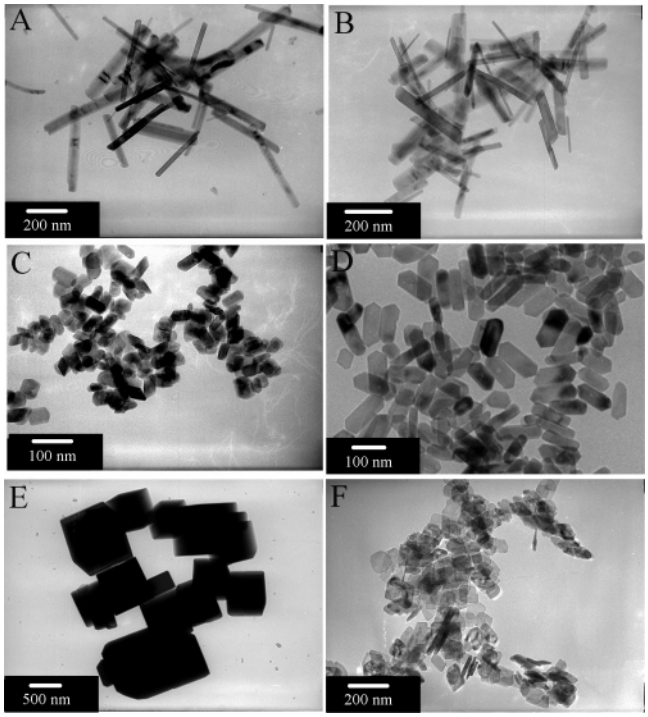

Figure 2. TEM images of the samples. (A) NaOH, pH 10; (B) NaOH, pH 12; (C) NaOH, pH 14; (D) 2.5 mol L^{-1} NaOH; (E) 5 mol L^{-1} NaOH; (F) NH_4OH, pH 10.

18 h at $[Sc^{3+}] = 0.025$ mol L^{-1} under various basic conditions have been determined (Figures 1 and 2 and Figures 1S and 2S and Table 1S in the Supporting Information). From Figure 1a, we see that α-ScOOH formed whatever the basicity value increasing from pH 10 to 2.5 mol L^{-1} NaOH. At pH 10, the lattice parameters of the as-synthesized α-ScOOH were a = 0.4802(8) nm, b = 1.0357(7) nm, and c = 0.3212(9) nm, (JCPDS No. 20-1035, *P*bnm). However, when the concentration of NaOH was further raised to 5 mol L^{-1}, only cubic $Sc(OH)_3$ with a lattice parameter of $a = 0.7906(4)$ nm (JCPDS No. 04-0389, *I*m3) was obtained. When NaOH was replaced by KOH, the structural evolution of the products with the system basicity was similar to that observed in the case of NaOH (Figure 1S and Table 1S in the Supporting Information), except that a mixed phase of cubic $Sc(OH)_3$ and α-ScOOH was obtained at 5 mol L^{-1} KOH. In the case of NH_4OH, Figure 1b shows the predominate presence of γ-ScOOH with lattice parameters of a = 0.404(2) nm, b = 1.296(9) nm, and c = 0.325(2) nm (JCPDS No. 17-941, *A*mam) within pH 10−12. The most intense peak was observed for the (020) reflection at $2\theta = 13.5°$, revealing the high crystallinity of γ-ScOOH and a strong ordering along the b axis of the unit cell.[23]

Figure 2 exhibits the TEM images of the ScOOH and $Sc(OH)_3$ samples. When NaOH was the base, α-ScOOH nanorods were obtained within pH 10−12 (Figure 2, parts A and B). At pH 10 and 12, the nanorods show sizes within (5−60) × (150−480) nm and (5−50) × (150−350) nm, respectively. When the basicity value was raised from pH 14 to 2.5 mol L^{-1} NaOH, hexagonal-like plates of about 45 and 87 nm formed, respectively (Figure 2, parts C and D). At 5 mol L^{-1} NaOH, 1 μm cube and cuboid-like $Sc(OH)_3$ crystallites were obtained (Figure 2E). The shape dependence of the products on the basicity in KOH medium resembled that in NaOH medium (Figure 2S and Table 1S in the Supporting Information), except that cubiod-like $Sc(OH)_3$ and hexagonal platelike α-ScOOH coexisted at 5 mol L^{-1} KOH and nanorod-like α-ScOOH formed only at pH 10. In the case of NH_4OH, the products obtained at pH 10 (Figure 2F) and 12 (Figure 2S-(f) in the Supporting Information) showed two types of shapes, i.e., a majority of lozenge-like plates with a size of 99 and 80 nm, plus a quite small portion of nanorods with sizes of (5−25) × (70−260) nm and 5 × 115 nm, respectively. According to a previous report on the hydrothermal synthesis of ScOOH using $ScCl_3$ and NH_4OH as the reactants by Ripert et. al.,[19] the lozenge-like plates were ascribed to γ-ScOOH, and the nanorods were attributed to Γ-ScOOH with different lattice parameters of a = 0.5150 nm, b = 0.4600 nm, and c = 0.3197 nm. Due to the fact that Γ-ScOOH was of trace amount and its XRD pattern severely overlapped with that of γ-ScOOH, the presence of Γ-ScOOH was not detected from the XRD patterns using NH_4OH (Figure 1b) in our work.

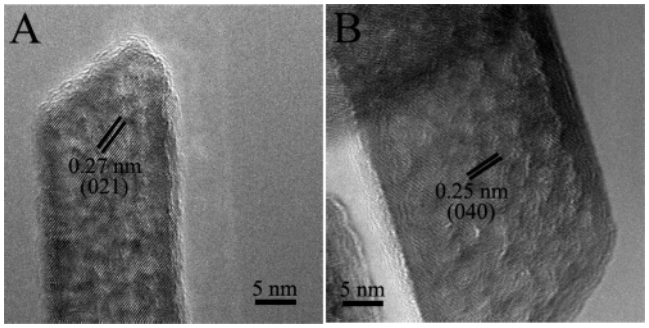

Figure 3. HRTEM images of the samples. (A) NaOH, pH 10; (B) NaOH, pH 14.

Figure 3 depicts the HRTEM images of the α-ScOOH nanocrystals prepared from NaOH medium. At pH 10, the rodlike product displays a clear (021) lattice fringe with an interplanar spacing of 0.27 nm (Figure 3A). At pH 14, the hexagonal-like plate product exhibits a clear (040) lattice fringe with an interplanar spacing of 0.25 nm (Figure 3B). These TEM results clearly reveal the single-crystalline nature of the nanocrystalline products. However, the surfaces and edges of the nanocrystals are rugged, indicating the existence of a high density of surface defects, which is likely a result of the strong hydroxylation/dehydroxylation interactions exerted during the hydrothermal processing under basic conditions.

3.2. Infrared and Raman Spectroscopy. Figure 4 shows the IR and Raman spectra of α-ScOOH, γ-ScOOH, and $Sc(OH)_3$ produced under different basic conditions. As is well-known, α-ScOOH and γ-ScOOH are isomorphous with α-AlOOH (diaspore) and γ-A1OOH (boehmite), respectively.[24,25] IR and Raman analyses for α-A1OOH and γ-A1OOH have been carried out,[26−29] according to which, the vibrational modes of the as-synthesized α-ScOOH, γ-ScOOH, and $Sc(OH)_3$ have been assigned (Table 2S in the Supporting Information). Four vibration modes, including hydroxyl stretching (ν(OH)), hydroxyl bending (δ(OH), hydroxyl deformation (γ(OH)), and Sc−O stretching, were observed (Table 2S in the Supporting Information). α-ScOOH, γ-ScOOH, and $Sc(OH)_3$ can be discriminated by their characteristic peaks in the Sc−O stretching region, either from IR or Raman data, and by those in the γ(OH) region from IR data. On IR spectra, in the Sc−O stretching region, the Sc−O−Sc symmetric stretching mode of α-ScOOH, γ-ScOOH, and $Sc(OH)_3$ is located at 460, 498, and 481 cm^{-1}, respectively, while their Sc−O−Sc symmetric bending mode appears at 310, 396, and 280 cm^{-1}, respectively. On Raman spectra, α-ScOOH, γ-ScOOH, and $Sc(OH)_3$ display the Sc−O−Sc symmetric stretching band at 429, 383, and 437 cm^{-1}, respectively, while they have Sc−O−Sc symmetric bending bands at 326, 281, and 304 cm^{-1}, respectively. In the γ(OH) region on IR spectra, the hydroxyl deformation mode

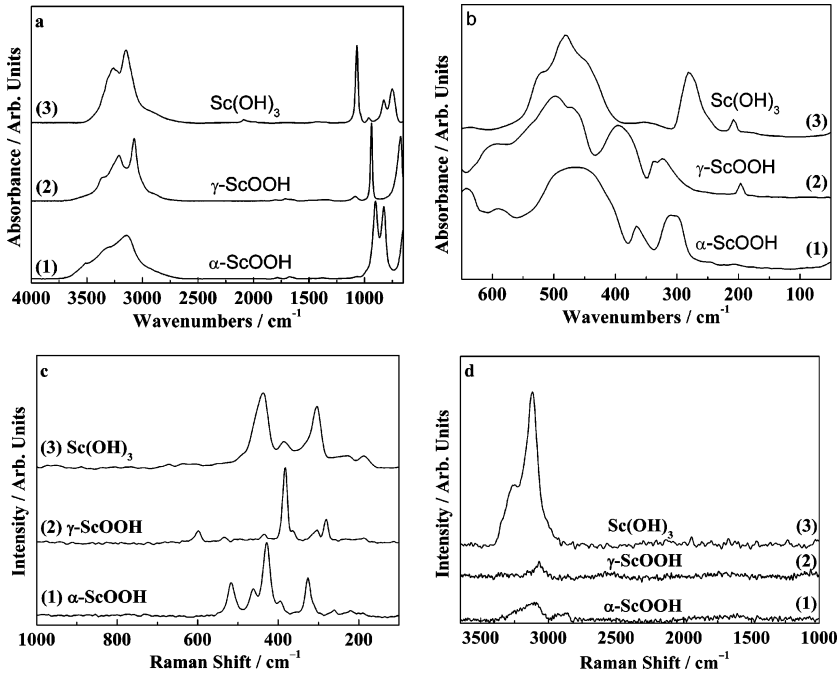

Figure 4. IR (a and b) and Raman (c and d) spectra of the samples. (1) α-ScOOH, NaOH, pH 10; (2) γ-ScOOH, NH_4OH, pH 10; (3) $Sc(OH)_3$, 5 mol L^{-1} NaOH.

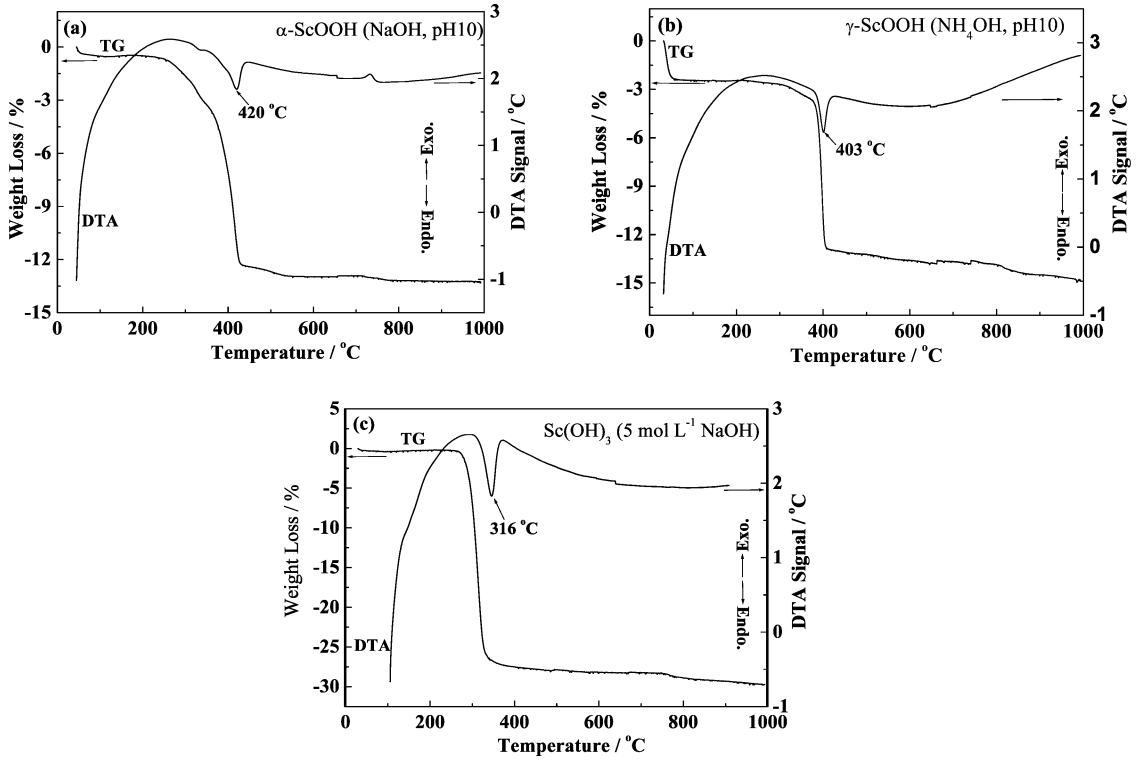

Figure 5. TG−DTA curves of the samples. (a) α-ScOOH, NaOH, pH 10; (b) γ-ScOOH, NH_4OH, pH 10; (c) $Sc(OH)_3$, 5 mol L^{-1} NaOH.

of α-ScOOH, γ-ScOOH, and $Sc(OH)_3$ appears at 826, 675, and 751 cm^{-1} (with a shoulder peak at 827 cm^{-1}), respectively.

3.3. Calcining Behavior. Figure 5 depicts the TG−DTA curves of α-ScOOH, γ-ScOOH, and $Sc(OH)_3$ obtained under different basic conditions. It is shown that α-ScOOH is converted into Sc_2O_3 with one-step weight loss of about 13% below 430 °C, with an endothermic reaction peak at 420 °C on the DTA curve (Figure 5a). γ-ScOOH transforms into Sc_2O_3 along with one-step weight loss of about 13% below 410 °C, displaying an endothermic reaction peak at 403 °C (Figure 5b). $Sc(OH)_3$ loses all hydroxyl groups in one-step below 332 °C with an endothermic reaction peak at about 316 °C, yielding Sc_2O_3 by a weight loss of around 28% (Figure 5c). According to the TG results, the temperatures for the conversion from ScOOH and $Sc(OH)_3$ into Sc_2O_3 follow the order of $Sc(OH)_3$ < γ-ScOOH < α-ScOOH.

Figure 6 shows the XRD patterns of samples obtained by the calcination of α-ScOOH, γ-ScOOH, and $Sc(OH)_3$ powders at 500 °C for 5 h. All the diffraction peaks can be attributed to cubic Sc_2O_3 (JCPDS No. 42-1463, *I*a3). However, the intensities of a few peaks for the two samples synthesized using NaOH at pH 10 and 14 are different from those of bulk Sc_2O_3 due to

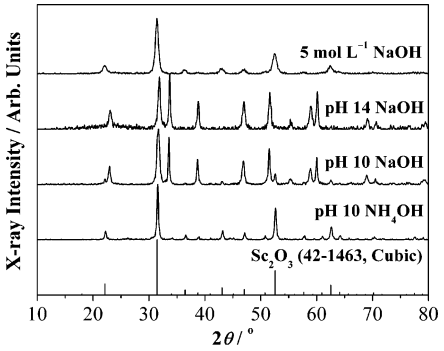

Figure 6. XRD patterns of the Sc_2O_3 powders prepared by calcination of ScOOH and $Sc(OH)_3$ at 500 °C for 5 h.

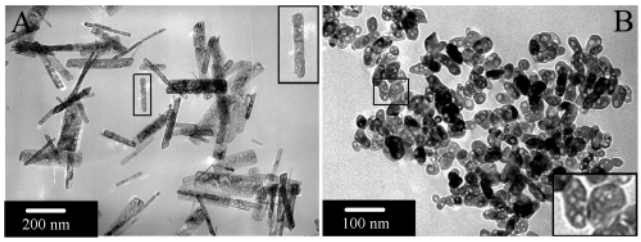

Figure 7. TEM images of the Sc_2O_3 powders prepared by calcination of ScOOH and $Sc(OH)_3$ at 500 °C for 5 h. (A) NaOH, pH 10; (B) NaOH, pH 14. (Inset was taken from the highlighted section.)

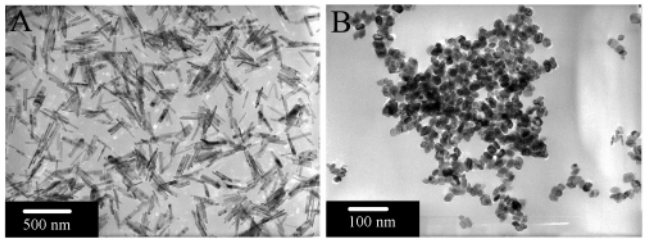

Figure 8. TEM images of the α-ScOOH samples prepared at 180 °C for 18 h at $[Sc^{3+}] = 0.075$ mol L^{-1}, using NaOH. (A) pH 11; (B) pH 14.

their large shape anisotropy, which can be verified by the TEM images shown in Figure 7. Since the conversion from α-ScOOH into Sc_2O_3 is pseudomorphic, the anisotropic crystalline shape of the particles was preserved throughout the calcination (compare Figures 7A and 2A and Figures 7B and 2C). However, in comparison with single-crystalline α-ScOOH, the rod and platelike Sc_2O_3 nanoparticles were made of very small Sc_2O_3 crystallites with many pores between them (insets in Figure 7), as a result of the strong dehydroxylation that occurred during the transformation from α-ScOOH into Sc_2O_3. From Figure 7, it is observed that the dehydroxlation effect also caused the surface of the as-calcined nanoparticles to become more rugged. A similar phenomenon, i.e., the oxide particles, showed unchanged shape, but significantly changed surface structure before and after calcination was observed in the transformation from γ-AlOOH into γ-Al_2O_3.[30]

3.4. FTIR Pyridine Adsorption and Surface Acidity. Through increasing the concentration of metal ions to 0.075 mol L^{-1}, we synthesized relatively uniform α-ScOOH nanocrystals at 180 °C for 18 h, using NaOH (Figure 8). The as-synthesized nanorods at pH 11 have a width in the range of 5.6−8.3 nm and a length in the range of 144−250 nm (Figure 8A), and the as-synthesized hexagonal-like plates at pH 14 have a size of 16−33 nm (Figure 8B); these two samples are named as **S1** and **S2**, respectively. By calcination of **S1** and **S2** at 700 °C for 2 h, samples **S3** and **S4** were obtained, respectively.

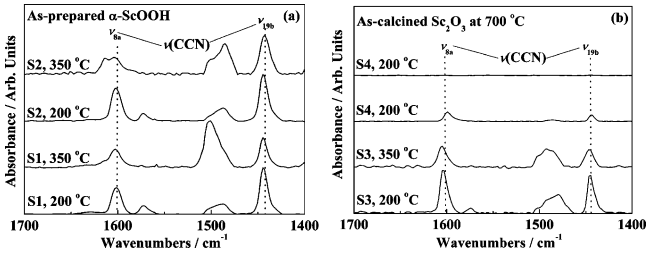

Figure 9. FTIR spectra of pyridine adsorption for (a) α-ScOOH and (b) Sc_2O_3 (calcined at 700 °C for 2 h) samples.

TABLE 1: Surface Area (*S*), Band Position, and Integral Absorbances Divided by the Weights of the Wafers (*A*) of the Samples

		S1	S2	S3	S4
S (m^2 g^{-1})		50	35	40	22
Lewis acid positions (cm^{-1})	200 °C	1445	1445	1445	1445
	350 °C	1445	1443	1447	
A (cm g^{-1})	200 °C	114	83	26	8
	350 °C	14	21	3	0

To test the surface acidity of samples **S1**, **S2**, **S3**, and **S4**, FTIR pyridine adsorption measurements were performed. As shown in Figure 9, the IR spectra of adsorbed pyridine showed characteristic absorption bands at 1660 and 1445 cm^{-1}, which correspond to the ν_{8a} and ν_{19b} modes of ring-breathing vibrations ν(CNN) of pyridine, indicating pyridine adsorption on Lewis acid sites presumably associated with scandium atoms.[31] The surface area, band position, and integral absorbances divided by the weights of the wafers for the four samples are listed in Table 1. The acidities of the Sc_2O_3 samples (**S3** and **S4**) are much smaller than those of the ScOOH samples (**S1** and **S2**) either at the desorption temperature of 200 °C or at 350 °C, indicating that the nanocrystals containing more hydroxyl species should have more Lewis acid sites. In addition, we can see that the sample with the larger surface area tends to have a stronger acidity. For a given sample, the acidity was considerably reduced with increasing the desorption temperature from 200 to 350 °C, which was also likely caused by the dehydroxylation effect. To summarize, the α-ScOOH nanorod sample (**S1**) had the largest amount of surface Lewis acid sites, possibly due its highest surface area (see Table 1).

4. Discussion

From the above results, we can see that that the nature and concentration of the bases significantly affected not only the phasic compositions but also the shapes of scandium hydrous oxides. In the following, we try to explain why various ScOOH polymorphs and $Sc(OH)_3$ with different shapes were formed under different basic conditions during hydrothermal crystallization, by considering the structural characteristics of γ-ScOOH, α-ScOOH, and $Sc(OH)_3$ and the hydrolytic behavior of Sc^{3+} ions in aqueous phase.

As is well-known, hydrous Sc_2O_3 exists in the forms of ScOOH and $Sc(OH)_3$.[24,25,32] ScOOH has at least three polymorphs; the familiar ones are metastable γ-ScOOH and stable α-ScOOH. Figure 10 shows the structural models of γ-ScOOH, α-ScOOH, and $Sc(OH)_3$ built up by CERIUS2 software.[33] γ-ScOOH comprises double layers of ScO_6 octahedra with oxygen sheets in a cubic close-packed (ccp) arrangement (Figure 10A), and the neighboring layers are combined via hydrogen bonding.[25] The stacking of the layers is such that the hydroxyls of one layer are located over the depression between the hydroxyl groups in the adjacent layer. The structure of

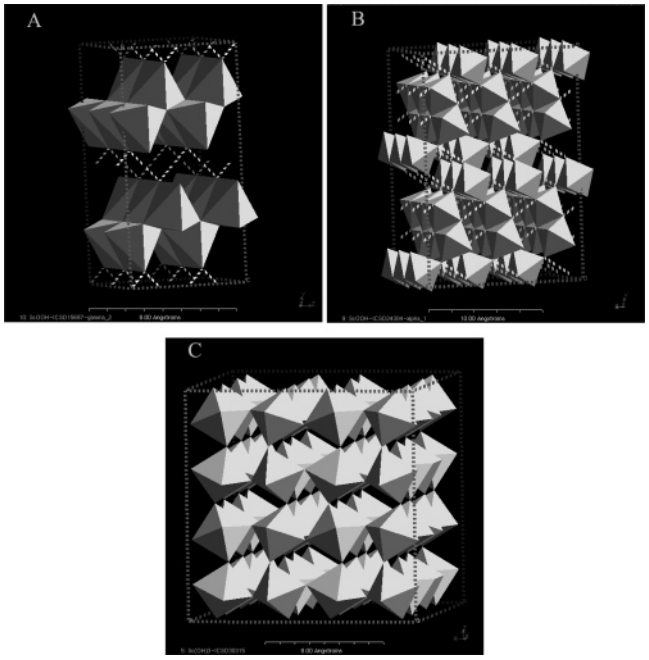

Figure 10. Structural models for (A) γ-ScOOH, (B) α-ScOOH, and (C) $Sc(OH)_3$. (A) $2 \times 1 \times 2$ unit cell; (B) $3 \times 2 \times 3$ unit cell; (C) $2 \times 2 \times 2$ unit cell.

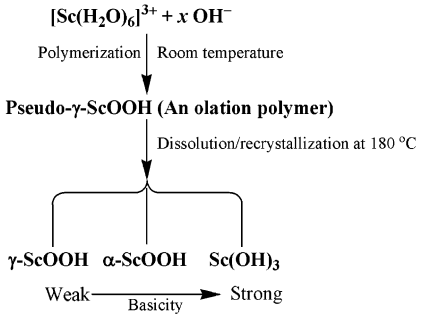

Figure 11. Schematic diagram for the formation of γ-ScOOH, α-ScOOH, and $Sc(OH)_3$.

α-ScOOH consists of infinite chains of ScO_6 octahedra with oxygen sheets in a hexagonal close-packed (hcp) arrangement, linked by hydrogen bonds (Figure 10B).[24] The hydroxyls are at the corners of the ScO_6 octahedra. $Sc(OH)_3$ consists of three-dimensional infinite chains of $Sc(OH)_6$ octahedra (Figure 10C), showing a face-body-centered cubic structure (fcc). Each Sc^{3+} is coordinated to six hydroxyls, and each hydroxyl is between two Sc^{3+} ions.[32]

In Figure 11, we show a schematic diagram accounting for the formation of γ-ScOOH, α-ScOOH, and $Sc(OH)_3$ during hydrothermal synthesis. This possible explanation is based on the olation ($M-OH + M-OH_2 \rightarrow M-OH-M + H_2O$ (M = metal ion)) and oxolation ($M-OH + M-OH \rightarrow M-O-M + H_2O$), as previously suggested in the synthesis of aluminum hydroxide by homogeneous precipitation.[34] Sc^{3+} usually displays a six-coordinate octahedral geometry in various coordination compounds.[35] In the present work, the Sc^{3+} cation in the stock solution is hydrated to form $[Sc(H_2O)_6]^{3+}$ in the presence of noncoordinating NO_3^- ions.[36] At room temperature, as a base is added into the stock solution to increase its pH value, $[Sc(H_2O)_6]^{3+}$ certainly will undergo strong hydrolysis to form $[Sc(OH)(H_2O)_5]^{2+}$, which is likely to further hydrolyze into $[Sc(OH)_2(H_2O)_4]^+$ species and into polynuclear species such as $[Sc_2(OH)_2(H_2O)_8]^{4+}$ via condensation of monomers.[23,36] The polynuclear species can cause further polymerization between itself and the monomers via olation and oxolation, leading to the formation of an olation polymer of pseudo-γ-ScOOH, as verified by the XRD patterns of the $Sc(OH)_3$ gels shown in Figure 1 and Figure 1S in the Supporting Information, whenever NaOH, NH_4OH, or KOH was used. This case is similar to the formation of pseudo-γ-AlOOH under basic conditions.[37]

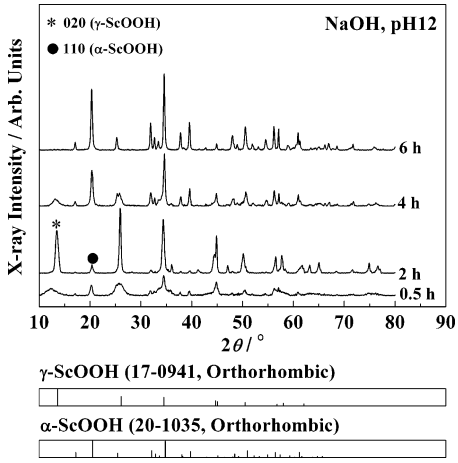

Figure 12. Time evolution of the XRD patterns for the samples prepared at 180 °C at pH 12 using NaOH.

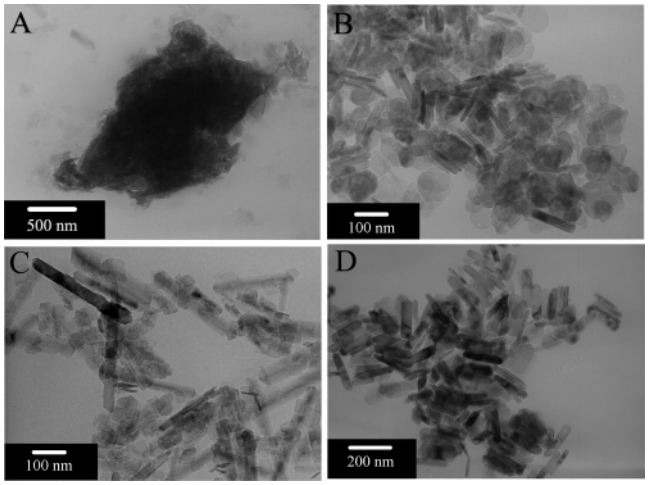

Figure 13. Time evolution of the TEM images for the samples prepared at 180 °C at pH 12 using NaOH. (A) 0.5 h; (B) 2 h; (C) 4 h; (D) 6 h.

When the pseudo-γ-ScOOH gels are subjected to hydrothermal treatment at 180 °C, ScOOH is likely to acquire high crystallinity via dissolution/recrystallization, which can be demonstrated by the results of the synthesis performed at pH 12 using NaOH (Figures 12 and 13). When the hydrothermal reaction went on for 0.5 h, the products contained a major portion of poorly crystallized γ-ScOOH gel and a small fraction of rodlike α-ScOOH (Figures 12 and 13A). With prolonging the reaction time from 0.5 to 4 h, the amount of α-ScOOH nanorods significantly increased along with improved crystallinity (Figure 12 and Figure 13, parts B and C). When the reaction time reached 6 h, pure α-ScOOH nanorods were obtained (Figures 12 and 13D). The gradual transformation from γ-ScOOH into α-ScOOH also confirmed the metastable nature of γ-ScOOH.

According to the above olation−oxolation process-based dissolution/recrystallization, under weakly basic conditions using NH_4OH, metastable γ-ScOOH was obtained. In its layered structure, both hydroxyl and oxygen bridges existed (Figure 10A). As NH_4OH was replaced by a much stronger base such as NaOH or KOH, stable α-ScOOH containing both hydroxyl

and oxygen bridges (Figure 10B) was obtained. Cubic $Sc(OH)_3$ with only hydroxyl bridges (Figure 10C) formed at a high base concentration (5 mol L^{-1}) due to the favored strong olation under the condition.

In general, the large structural anisotropy of an inorganic compound and its high chemical potential in solution are two main driving forces for the formation of anisotropic nanocrystals during the nontemplate synthesis.[8,38,39] We attempted to use this orderliness to explain the influences of the bases (nature and concentration) on the growth of our ScOOH and $Sc(OH)_3$ products in various shapes. Both γ-ScOOH and α-ScOOH are orthorhombic and have large structural anisotropy, so they can form anisotropic nanocrystals easily. Under weak basic conditions using NH_4OH, γ-ScOOH appeared in thin platelike morphology within pH 10−12 due to its layered structure.[23] Similar platelike morphology is usually observed for γ-AlOOH,[30] which is isostructural to γ-ScOOH.

Under relatively strong basic conditions, it is rational that the olation−oxolation process leads to the coexistence of both ScOOH and $Sc(OH)_3$ species in reacting solutions during synthesis, and strong olation enhances the concentration of $Sc(OH)_3$. In the case of NaOH, within pH 10−12, the olation would be rather weak, which must favor a high concentration of α-ScOOH species rather than $Sc(OH)_3$ and, thus, its high chemical potential in water solution. Under this condition, α-ScOOH nanorods formed by crystal growth along a preferred orientation, driven by the high chemical potential. When the basicity value of the reaction medium was increased from pH 14 to 2.5 mol L^{-1} NaOH, the olation was significantly enhanced and the chemical potential of α-ScOOH was considerably reduced due to its remarkable concentration decrease. Under this condition, less anisotropic α-ScOOH in hexagonal platelike morphology formed. As the base concentration was further increased to 5 mol L^{-1} NaOH, α-ScOOH totally transformed into cubic $Sc(OH)_3$, as a result of very strong olation in the existence of a rather high concentration of OH^- species. Due to its structural isotropy (Figure 10C), micrometer-sized $Sc(OH)_3$ was obtained in cube and cuboid-like shapes. The above explanations for the shape evolution of the products in NaOH medium are also suitable in the case of KOH medium.

5. Conclusions

Under various basic conditions using NaOH, NH_4OH, or KOH, nanostructured scandium hydrous oxides were hydrothermally synthesized at 180 °C for 18 h. The nature and concentration of the bases remarkably influenced the phasic composition, the texture behavior (shape and size), and surface state of the hydrothermal products. During the hydrothermal processing, the shape evolution of the crystalline products also depended heavily upon their crystal structures. When using a weak base (NH_4OH) within pH 10−12, we obtained nanosized γ-ScOOH lozenge-like plates as the main products. When using a strong base (NaOH or KOH), we obtained α-ScOOH nanorods, nanosized hexagonal-like plates, and cubic $Sc(OH)_3$ cubes/cuboids in turn across the basicity value varied from pH 10 to 5 mol L^{-1}. With the help of the structural models constructed for γ-ScOOH, α-ScOOH, and $Sc(OH)_3$, we found that the above dependence of crystalline shapes as well as the crystal structures upon bases could be explained by an olation−oxolation process based on a dissolution/recrystallization mechanism. Cubic Sc_2O_3 with nearly sustained crystalline shape was prepared from nanostructured ScOOH via calcination at 500 °C. Many Lewis acid sites were found on the surfaces of some nanostructured α-ScOOH and Sc_2O_3 samples (calcined at 700 °C). The α-ScOOH nanorod sample showed the strongest Lewis acidity due to its highest surface area. In conclusion, we expect the as-prepared nanosized ScOOH and Sc_2O_3 to be promising candidate materials for novel catalytic applications (particularly in acid−base-catalyzed reactions). This research also provides useful clues for the synthesis of MOOH (M = Al, Fe, Mn, Cr, Co, Ga, In, Yb) and corresponding oxide nanostructures for many other important applications.[40]

Acknowledgment. We gratefully acknowledge the financial aid from NSFC (Nos. 20171003, 20221101, and 20490210) and the Founder Foundation of PKU.

Supporting Information Available: Phases, crystalline shapes, and sizes of the samples prepared using different bases (Table 1S); IR and Raman spectral data assigned to vibrational modes for ScOOH and $Sc(OH)_3$ (Table 2S); XRD patterns of the samples prepared using KOH and the $Sc(OH)_3$ gel prepared at pH 10 in air at room temperature (Figure 1S); TEM images of the samples prepared using KOH or NH_4OH (Figure 2S); XRD patterns of the samples prepared at pH 5 and pH 8 using NH_4OH (Figure 3S); TEM images of the samples prepared at pH 5 and pH 8 using NH_4OH (Figure 4S). This material is available free of charge via the Internet at http://pubs.acs.org.

References and Notes

(1) Tjong, S. C.; Chen, H. *Mater. Sci. Eng., R* **2004**, *45*, 1.
(2) Cushing, B. L.; Kolesnichenko, V. L.; O'Connor, C. J. *Chem. Rev.* **2004**, *104*, 3893.
(3) Fernandez-Garcia, M.; Martinez-Arias, A.; Hanson, J. C.; Rodriguez, J. A. *Chem. Rev.* **2004**, *104*, 4063.
(4) Hu, J. T.; Odom, T. W.; Lieber, C. M. *Acc. Chem. Res.* **1999**, *32*, 435.
(5) Xia, Y. N.; Yang, P. D.; Sun, Y. G.; Wu, Y. Y.; Mayers, B.; Gates, B.; Yin, Y. D.; Kim, F.; Yan, H. Q. *Adv. Mater.* **2003**, *15*, 353.
(6) Wu, Y. Y.; Yan, H. Q.; Huang, M.; Messer, B.; Song, J. H.; Yang, P. D. *Chem. Eur. J.* **2002**, *8*, 1260.
(7) Patzke, G. R.; Krumeich, F.; Nesper, R. *Angew. Chem., Int. Ed.* **2002**, *41*, 2446.
(8) Wang, X.; Li, Y. D. *Angew. Chem., Int. Ed.* **2002**, *41*, 4790.
(9) Xu, A. W.; Fang, Y. P.; You, L. P.; Liu, H. Q. *J. Am. Chem. Soc.* **2003**, *125*, 1494.
(10) Wu, C. F.; Qin, W. P.; Qin, G. S.; Zhao, D.; Zhang, J. S.; Huang, S. H.; Lu, S. Z.; Liu, H. Q.; Lin, H. Y. *Appl. Phys. Lett.* **2003**, *82*, 520.
(11) Yada, M.; Mihara, M.; Mouri, S.; Kuroki, M.; Kijima, T. *Adv. Mater.* **2002**, *14*, 309.
(12) Wei, Z. G.; Sun, L. D.; Liao, C. S.; Yin, J. L.; Jiang, X. C.; Yan, C. H.; Lu, S. Z. *J. Phys. Chem. B* **2002**, *106*, 10610.
(13) Stouwdam, J. W.; van Veggel, F. C. J. M. *Nano Lett.* **2002**, *2*, 733.
(14) Riwotzki, K.; Meyssamy, H.; Schnablegger, H.; Kornowski, A.; Haase, M. *Angew. Chem., Int. Ed.* **2001**, *40*, 573.
(15) Otsuka, K.; Zhang, Q. H.; Yamanaka, I.; Tono, H.; Hatano, M.; Kinoshita, H. *Bull. Chem. Soc. Jpn.* **1996**, *69*, 3367.
(16) Zhang, Y. W.; Yang, Y.; Jin, S.; Tian, S. J.; Li, G. B.; Jia, J. T.; Liao, C. S.; Yan, C. H. *Chem. Mater.* **2001**, *13*, 372.
(17) Rainer, F.; Lowdermilk, W. H.; Milam, D.; Hart, T. T.; Lichtenstein, T. L.; Carniglia, C. K. *Appl. Opt.* **1982**, *21*, 3685.
(18) Grosso, D.; Sermon, P. A. *J. Mater. Chem.* **2000**, *10*, 359.
(19) Ripert, V.; Hubert-Pfalzgraf, L. G.; Papiernik, R.; Belleville, P.; Floch, H. *J. Mater. Chem.* **2001**, *11*, 1880.
(20) Li, J.; Ikegami, T.; Mori, T.; Yajima, Y. *J. Am. Ceram. Soc.* **2003**, *86*, 1493.
(21) Langford, J. I. *J. Appl. Crystallogr.* **1971**, *4*, 259.
(22) Langford, J. I. *J. Appl. Crystallogr.* **1973**, *6*, 190.
(23) Li, J.; Ikegami, T.; Mori, T.; Yajima, Y. *J. Mater. Res.* **2003**, *18*, 1149.
(24) Christensen, A. N.; Jensen, S. J. *Acta Chem. Scand.* **1967**, *21*, 121.
(25) Milligan, W. O.; Mcatee, J. L. *J. Phys. Chem.* **1956**, *60*, 273.
(26) Frost, R. L.; Kloprogge, J. T.; Russell, S. C.; Szetu, J. *Appl. Spectrosc.* **1999**, *53*, 572.
(27) Frost, R. L.; Kloprogge, J. T.; Russell, S. C.; Szetu, J. *Appl. Spectrosc.* **1999**, *53*, 829.

(28) Ruan, H. D.; Frost, R. L.; Kloprogge, J. T.; Duong, L. *Spectrochim. Acta, Part A* **2002**, *58*, 265.

(29) Ruan, H. D.; Frost, R. L.; Kloprogge, J. T. *J. Raman Spectrosc.* **2001**, *32*, 745.

(30) Paglia, G.; Buckley, C. E.; Rohl, A. L.; Hart, R. D.; Winter, K.; Studer, A. J.; Hunter, B. A.; Hanna, J. V. *Chem. Mater.* **2004**, *16*, 220.

(31) Little, L. H. *Infrared Spectra of Adsorbed species*; Academic Press: London, 1966; pp 193−198.

(32) Schubert, K.; Seitz, A. *Z. Anorg. Chem.* **1948**, *256*, 226.

(33) Accelrys Software Inc. *Cerius^2 2.4.6: http://www.accelrys.com/cerius2/*; Accelrys Software Inc.: San Diego, CA, USA, 2001.

(34) Nagai, H.; Hokazono, S.; Kato, A. *Br. Ceram. Trans. J.* **1991**, *90*, 44.

(35) Meehan, P. R.; Aris, D. R.; Willey, G. R. *Coord. Chem. Rev.* **1999**, *181*, 121.

(36) Baes, C. F.; Mesmer, R. E. *The Hydrolysis of Cations*; John Wiley & Sons: New York, 1976; pp 123−128.

(37) Bye, G. C.; Robinson, J. G. *Kolloid-Z.* **1964**, *198*, 53.

(38) Peng, Z. A.; Peng, X. G. *J. Am. Chem. Soc.* **2001**, *123*, 1389.

(39) Zhang, Y. W.; Yan, Z. G.; You, L. P.; Si, R.; Yan, C. H. *Eur. J. Inorg. Chem.* **2003**, *22*, 4099.

(40) (a) Hicks, R. W.; Pinnavaia, T. J. *Chem. Mater.* **2003**, *15*, 78. (b) Wang, X.; Chen, X. Y.; Gao, L. S.; Zheng, H. G.; Ji, M. R.; Tang, C. M.; Shen, T.; Zhang, Z. D. *J. Mater. Chem.* **2004**, *14*, 905. (c) Huang, C.-C.; Yeh, C.-S.; Ho, C.-J. *J. Phys. Chem. B* **2004**, *108*, 4940.